International Journal of Power Electronics and Drive System (IJPEDS)
Vol. 17, No. 1, March 2026, pp. 168~179
ISSN: 2088-8694, DOI: 10.11591/ijpeds.v17.i1.pp168-179

Design and improvement of dynamic performance of solar-powered BLDC motor for electric vehicles in agricultural applications

Savitri Medegar, M. Sasikala
Department of Electrical and Electronics Engineering, Sharnbasva University, Kalaburagi, India

Article Info

Article history:

Received Aug 6, 2025
Revised Dec 22, 2025
Accepted Jan 23, 2026

Keywords:

BLDC motor
Boost converter
MATLAB/Simulink
MPPT
PI controller
PV system

ABSTRACT

One of the most pressing environmental problems is the rapid increase in the production of greenhouse gases by transportation vehicles. This paper looks into SPEVs, or solar-powered electric vehicles. The answer to the problems of transportation-related pollution and fuel usage. In an electric vehicle, the power comes from a battery that may be charged by solar panels or any other external power source. By making use of the perturb and observe (P&O) maximum power point tracking (MPPT) controller, one can achieve maximum power. The DC voltage that the photovoltaic module produces is amplified when it is fed into a voltage source inverter (VSI) via this enhanced output. The tool for the job here is a buck-boost converter. To power their wheels, EVs rely on brushless direct current (BLDC) motors and variable speed inverters (VSIs), which transform DC power from solar panels into AC power. We compare the efficiency of electric vehicles (EVs) attained by raising converter voltages and battery state of charge (SoC) using a PI controller, and we look at the performance of photovoltaic (PV) and brushless linear direct current (BLDC) motors. We use MATLAB/Simulink to do the validation.

Corresponding Author:

Savitri Medegar
Department of Electrical and Electronics Engineering, Sharnbasva University
Kalaburagi 585103, India
Email: savtri.m@sharnbasvauniversity.edu.in

NOMENCLATURE

I : Output current of PV cell	R_s, R_{sh} : Series and shunt resistances, respectively
V : Output voltage of PV cell	I_{sh} : Current due to shunt resistance
I_{ph} : Photo-generated current	C : Elementary charge 1.6×10^{-19}
I_D : Diode current	K : Boltzmann constant 1.38×10^{-23}J/K
I_{sh} : Shunt current	γ : Idealist factor
V_{oc} : Open circuit voltage	T : Cell temperature
I_{rs} : Diode reverse saturation current (I_0)	T_r : Reference temperature
I_{csc} : Cell saturation current at T_{rt}	K_I : Short circuit current temperature coefficient at I_{scr}
I_{scr} : Short circuit current	N_{SC} : The number of solar cells in the series in the solar module
V_{dc} : Diode voltage	N_{CP} : the number of solar cells in parallel in the solar module

1. INTRODUCTION

Combustion engines, which power all contemporary modes of transportation, are extremely harmful to the environment due to the greenhouse gases they emit. Regardless, there have been vast shifts in transportation

technology, with a focus on electric vehicles (EVs) replacing internal combustion engines. The high price and limited range of electric vehicles are two reasons why many are skeptical about new transportation technology [1]. Electric vehicles that rely on solar power generally operate on energy that is generated by the sun. There will be no pollution with SPEVs. A few key advantages of solar-powered electric vehicles (SPEVs) include: being able to collect energy from the sun, reusing and recycling that energy through regenerative braking, minimizing mechanical losses, producing zero pollutants, being easy to install and operate, and being fault-tolerant as a result of their improved energy efficiency [2]-[4]. The fact that electric vehicles require recharging every 60 to 70 kilometers driven is a downside that limits their market status and personal usage. But for now, a lot of people charge their electric cars in parking lots and at roadside stations. Recharging the battery of an EV typically takes between two and three hours, though this can vary greatly depending on the battery's capacity. The work [5] provides a novel mechanism that automatically charges the battery system in order to address the problem. By 2030, electric vehicles are likely to replace all internal combustion engine vehicles. Recently, a number of DC solar-powered electric vehicles have been produced and studied [6]. Solar panels are placed for the extraction of solar energy. Solar panels used in EV needs storage device to store electrical energy [7]. A control algorithm can approximate the nickel-metal hydride battery packs used in electric vehicles [8]. Traction battery packs are charged using a high-frequency AC-DC converter integrated with an electromagnetic interference filter [9]. Numerous studies have been conducted to increase the efficiency of PV systems. Various strategies are used to track the maximum power point from PV modules in order to obtain higher efficiency, and also numerous consumer-facing products that use these techniques are on the market [10], [11]. The most feasible and effective alternative renewable energy source is solar power [12].

The expense, energy limitations, and low power density of SPEVs make them impractical for usage in real-world scenarios [13]. The batteries in electric vehicles (EVs) and plug-in hybrid electric vehicles (PHEVs) typically consist of numerous cells connected in parallel or series. Various operational conditions and manufacturing inconsistencies can reduce the usable energy of these batteries [14], [15]. The design of an SPEV is presented in this research study, and MATLAB is used to simulate its operation. The maximum power point tracking (MPPT) technique is used to get a larger amount of electricity from the panels in a variety of scenarios [16]. The buck-boost converter receives the solar panel output power and raises the voltage to a predetermined level so that the battery can be charged via the charge controller. The charging process is terminated based on the battery's status to prevent deep drain and overcharging. In automotive applications, brushless direct current (BLDC) motors are powered by a 3-ϕ voltage source inverter.

2. METHOD

This work focuses on the integration of renewable energy sources for charging electric vehicles. The workflow diagram of the methodology illustrates the operation of the SPEV system. The processes involved in the suggested methodology are shown in Figure 1.

2.1. Solar cell

A basic equivalent circuit model of a photovoltaic array, constructed from series and parallel connections of PV solar cells. PV cell voltage is directly proportional to photocurrent, which is primarily determined by solar irradiation strength and load current [17]. Considering a single solar cell in Figure 2, a PV module can be modeled by using a current source, a diode, and two resistors. The equivalent circuit of a PV cell consists of photo current (Iph), a diode, series resistance (Rs), and parallel resistance (Rsh). The photo current is anti-parallel with the diode [18].

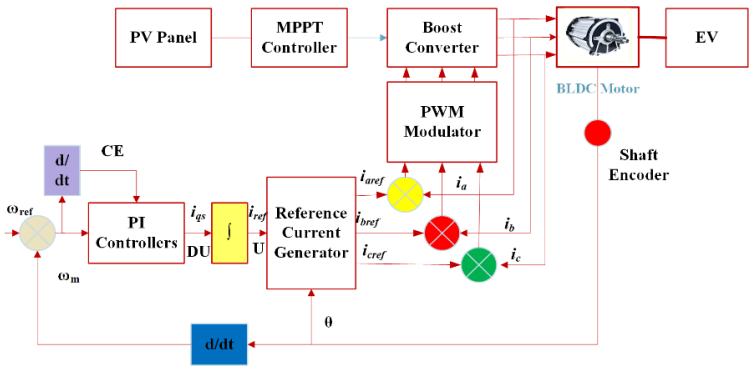

Figure 1. The block diagram of speed regulation in the BLDC motor

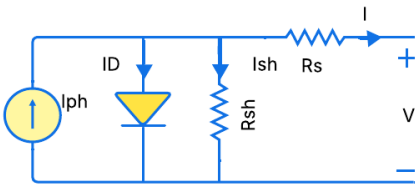

Figure 2. Single solar cell equivalent circuit

Mathematical modelling of a solar cell in MATLAB:

$$I=I_{ph}-I_D-I_{sh} \quad (1)$$

$$I=I_{ph}-I_{crs}\{\exp(AV_D-1)\}-\frac{V_{dc}}{R_{sh}} \quad (2)$$

$$A=\frac{C}{NYKT} \quad (3)$$

$$V_D=V+IR_s \quad (4)$$

$$I_{crs}=I_{csc}\left[\frac{T}{T_{rt}}\right]^3 \quad (5)$$

$$I_{ph}=[I_{sc}+K_i(T-T_{rt})]\frac{1}{1000} \quad (6)$$

Applying Kirchhoff's current law in the model shown in Figure 2. The current divided through the diode is:

$$I_D=I_o\left[\exp\frac{C(V+IR_{sr})}{mkT}\right]-1 \quad (7)$$

Where I_o = diode saturation current, m = diode quality factor, and T_c = absolute temperature of cell (K).

$$I=I_{ph}-I_o\left(\exp\left[\frac{C(V+IR_s}{mkT}\right]-1\right)-\frac{(V+IR_s)}{R_{sh}} \quad (8)$$

The maximum output of the PV panel is as given (9)-(12). The current at the maximum power point, I_{mpp} is (9).

$$I_{mpp}=I_{ph}-I_o\left(\exp\left[\frac{C(V_{mpp}+I_{mpp}R_s}{mkT}\right]-1\right)-\frac{(V_{mpp}+I_{mpp}R_s)}{R_{sh}} \quad (9)$$

Where I_{mpp}= maximum panel current, V_{mpp} = maximum panel voltage, and P_{max} = maximum power point by PV panel.

$$P_{max}=V_{mpp}\left\{I_{ph}-I_o\left(\exp\left[\frac{C(V_{mpp}+I_{mpp}R_r}{mkT}\right]-1\right)-\frac{(V_{mpp}+I_{mpp}R_s)}{R_{sh}}\right\} \quad (10)$$

The Vout of the panel is given as (11) and (12).

$$V=N_{sc}(V_{dc}-R_sI) \quad (11)$$

$$I=I_{ph}-I_{dc}-I_{sh} \quad (12)$$

The "Photovoltaic generator (PVG)" or "PV array" is composed of many PV Panels connected in N_{sp}-PV modules in series, N_{pp}-PV modules in parallel panels to achieve desired values of voltage and current.

$$V_{pvm}=N_{sc}\times N_{sp}\times V_p \quad (13)$$

$$I_{pvm}=N_{pc}\times N_{pp}\times I_p \quad (14)$$

Where V_{pvm} and I_{pvm} are generated output voltage, current at the PV array module. Then we have to compute PV array voltage and current, which are V_{pva}, I_{pva} and P_{pva}. Where:

$$V_{pva}=V_{pvm}\times N_{sc} \quad (15)$$

$$I_{pva}=I_{pvm}\times N_{pc} \quad (16)$$

$$P_{pva}=V_{pva}\times I_{pva} \quad (17)$$

2.2. Perturb and observe the MPPT method

An MPPT device measures the highest power output from the PV modules, transforms it into voltage, and then supplies the battery with the maximum current required for charging. The conversion rate of current MPPTs is 90–93% efficient. During summer, power gains are typically between 20% and 45%, whereas wintertime power gains range from 10% to 15%. The real power boost, however, is dependent on a number of variables, including battery charge and temperature [19]. Therefore, MPPT uses a perturb and observe (P&O) algorithm to maximize the power output from PV panels in order to run the load. The MPPT P&O algorithm is depicted in Figure 3. The P&O operates on the basis of comparing the latest power with the previous power in order to alter the voltage levels.

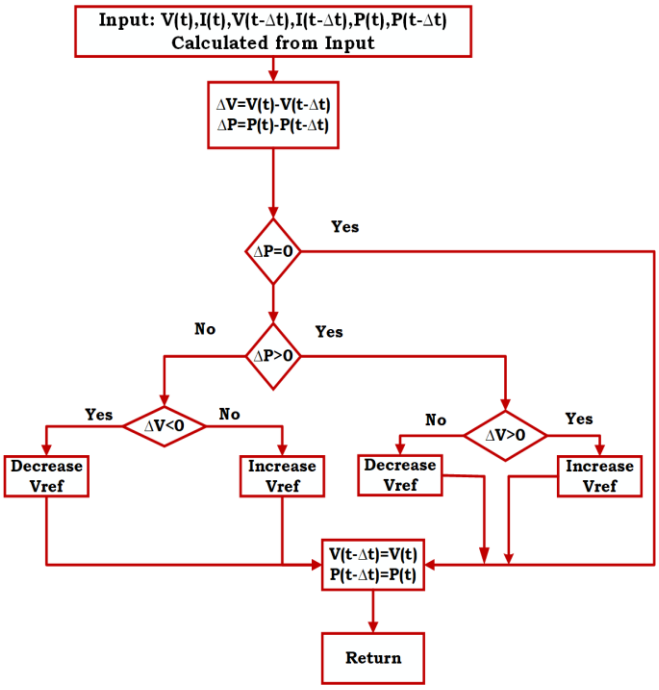

Figure 3. Flow chart of the MPPT algorithm

3. BRUSHLESS DC MOTOR (BLDC MOTOR)

A BLDC motor converts electrical energy into mechanical energy. Among various types of motors, BLDC motors are particularly versatile due to their high efficiency, ease of control, lightweight design, and simplicity. One key advantage of BLDC motors over others is their power-saving capability. The motor's rotor and stator magnetic fields operate at the same frequency, and the absence of brushes enhances efficiency and extends the motor's lifespan. Additionally, BLDC motors experience fewer losses and offer superior starting torque [20]. Because of the above-listed advantages, three-phase BLDC motors are increasingly being used in electric vehicles.

3.1. Modelling of BLDC motor

Figure 4 shows the overall setup for the speed regulation of the PV-fed BLDC motor. A BLDCM's rotor consists of three stator windings coiled around a permanent magnet. It is possible to disregard rotor

currents due to the high resistance of magnets and stainless steel. At this time, damper winding modeling is not provided. Solving the equation for a three-winding circuit is all that's needed to find the phase variables [21]:

$$\begin{bmatrix} V_{ast} \\ V_{bst} \\ V_{cst} \end{bmatrix} = \begin{bmatrix} R_{st} & 0 & 0 \\ 0 & R_{st} & 0 \\ 0 & 0 & R_{st} \end{bmatrix} \begin{bmatrix} i_{ast} \\ i_{bst} \\ i_{cst} \end{bmatrix} + \frac{d}{dt} \begin{bmatrix} L_{aa} & L_{ab} & L_{bc} \\ L_{ba} & L_{bb} & L_{bc} \\ L_{ca} & L_{cb} & L_{cc} \end{bmatrix} \begin{bmatrix} i_{ast} \\ i_{bst} \\ i_{cst} \end{bmatrix} + \begin{bmatrix} e_a \\ e_b \\ e_c \end{bmatrix} \tag{18}$$

where Rs stands for stator resistance and vast, vbst, and vcst denote stator phase voltages. These three current i_{cst}, i_{ast}, and i_{bst} flow through the stator in three phases. The phases L_{aa}, L_{bb}, and L_{cc} each have their unique self-inductance. Labor, LBC, and Lac are the phase-to-phase inductances. Electromotive pressures are linked to phases E_a, E_b, and E_c. It has been presumed that the resistance of each winding is equivalent. Additionally, it is believed that the lack of a visible rotor causes the rotor reluctance to remain constant regardless of the angle.

The (19) and (20) are substituted for (18) to form the PMBDCM model.

$$L_{aa} = L_{aa} = L_{aa} = L \tag{19}$$

$$L_{aa} = L_{ba} = L_{ac} = L_{ca} = L_{bc} = L_{cb} = M \tag{20}$$

$$\begin{bmatrix} V_{ast} \\ V_{bst} \\ V_{cst} \end{bmatrix} = \begin{bmatrix} R_{st} & 0 & 0 \\ 0 & R_{st} & 0 \\ 0 & 0 & R_{st} \end{bmatrix} \begin{bmatrix} i_{ast} \\ i_{bst} \\ i_{cst} \end{bmatrix} + \frac{d}{dt} \begin{bmatrix} L & M & M \\ M & L & M \\ M & M & L \end{bmatrix} \begin{bmatrix} i_{ast} \\ i_{bst} \\ i_{cst} \end{bmatrix} + \begin{bmatrix} e_a \\ e_b \\ e_c \end{bmatrix} t \tag{21}$$

The source voltages, which may be thought of as v_{ast}, v_{bst}, and v_{cst}

$$v_{ast} = v_{ao} - v_{no}, v_{bst} = v_{bo} - v_{no} \; and \; v_{cst} = v_{co} - v_{no} \tag{22}$$

The zero-reference potential at the middle of the DC connection is represented by vno, while the three-phase and neutral voltages are v_{ao}, v_{bo}, and v_{co}, respectively. The stator phase currents are limited to be balanced.

$$i_{ast} + i_{bst} + i_{cst} = 0 \tag{23}$$

Because of this, the inductance grid is made easier to understand.

$$M_{ib} + M_{ic} = -M_{ia} \tag{24}$$

Consequently, in the realm of state space.

$$\begin{bmatrix} V_{ast} \\ V_{bst} \\ V_{cst} \end{bmatrix} = \begin{bmatrix} R_{st} & 0 & 0 \\ 0 & R_{st} & 0 \\ 0 & 0 & R_{st} \end{bmatrix} \begin{bmatrix} i_{ast} \\ i_{b}st \\ i_{cst} \end{bmatrix} + \frac{d}{dt} \begin{bmatrix} L-M & 0 & 0 \\ 0 & L-M & 0 \\ 0 & 0 & L-M \end{bmatrix} \begin{bmatrix} i_{ast} \\ i_{bst} \\ i_{cst} \end{bmatrix} + \begin{bmatrix} e_a \\ e_b \\ e_c \end{bmatrix} \tag{25}$$

Traditionally, it has been believed that the back EMFs (e_a, e_b, and e_c) exhibit a trapezoidal wave coming from (26).

$$\begin{bmatrix} e_a \\ e_b \\ e_c \end{bmatrix} = \omega_m \lambda_m \begin{bmatrix} f_{as}(\theta_r) \\ f_{bs}(\theta_r) \\ f_{cs}(\theta_r) \end{bmatrix} \tag{26}$$

Here, ω_m denotes the angular rotor speed in radians per second, m, the flux linkage, and r, the rotor position in radians. With a maximum magnitude of ±1, the functions $f_{as}(\theta_r)$, $f_{bs}(\theta_r)$ and $f_{cs}(\theta_r)$ are the same as e_a, $e_b$and e_c,. Due to their trapezoidal shape, induced emfs lack sharp corners. The derivatives of flux connections generate electromagnetic fields, which are continuous functions. A smooth and edge-free flux density function is the result of fringes [23].

The electromagnetic torque, according to Newton, is (27).

$$T_e = e_a i_a + e_b i_b + e_a i_c \tag{27}$$

The inertia is defined as (28).

$$J = J_m + J_l \tag{28}$$

Load torque T_l, inertia (J), and friction coefficient (B) are all variables in (29).

$$J\frac{d\omega_m}{dt} + B\omega_m = (T_e - T_l) \tag{29}$$

The speed-position relationship of the electrical rotor.

$$\frac{d\theta_r}{dt} = \frac{p}{2}\omega_m \tag{30}$$

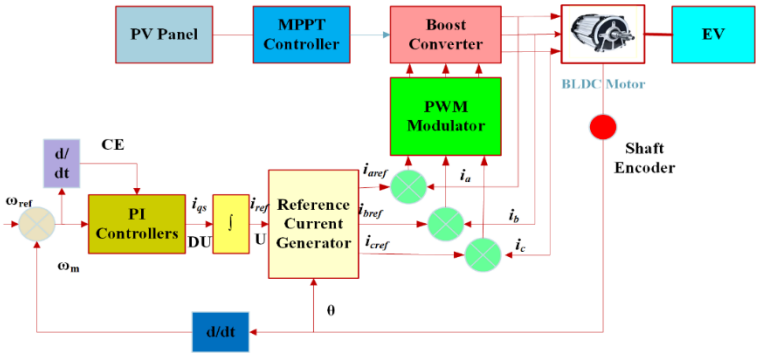

Figure 4. General configuration of the speed controller of the PV-fed BLDC motor

Despite its typically insignificant size, the damping coefficient B affects the system. The equation "θ_r" which represents the rotor location, is repeated every 2π cycles. To keep the drive efficient and prevent a voltage imbalance, one must consider the potential of the point of neutrality in relation to zero potential (vno). We obtain by changing the VI equation from (25) to (24).

$$v_{a0} + v_{b0} + v_{c0} - 3v_{n0} = R_s(i_a + i_b + i_c) + (L - M)(pi_a + pi_b + pi_c) + (e_a + e_b + e_c) \tag{31}$$

Substituting (23) in (31) yields the following:

$$v_{a0} + v_{b0} + v_{c0} - 3v_{n0} = (e_a + e_b + e_c)$$

Thus:

$$v_{n0} = [v_{a0} + v_{b0} + v_{c0}] - (e_a + e_b + e_c)]/3 \tag{32}$$

There is a connection between the differential (25), (29), and (30). defines the model by the production use of variables that are self-governing $i_{ast}, i_{bst}, i_{cst}, \omega_m$ and θ_r. Combining all relevant equations yields (33).

$$\dot{x} = Ax + Bu + Ce \tag{33}$$

Where:

$$x = [i_{ast} \quad i_{bst} \quad i_{cst} \quad \omega_m \quad \theta_r]^t \tag{34}$$

$$A = \begin{bmatrix} -\frac{R_{st}}{L-M} & 0 & 0 & -\frac{\lambda_m}{J}f_{as}(\theta_r) & 0 \\ 0 & -\frac{R_{st}}{L-M} & 0 & -\frac{\lambda_m}{J}f_{bs}(\theta_r) & 0 \\ 0 & 0 & -\frac{R_{st}}{L-M} & -\frac{\lambda_m}{J}f_{cs}(\theta_r) & 0 \\ \frac{\lambda_m}{J}f_{as}(\theta_r) & \frac{\lambda_m}{J}f_{bs}(\theta_r) & \frac{\lambda_m}{J}f_{cs}(\theta_r) & -\frac{B}{J} & 0 \\ 0 & 0 & 0 & \frac{P}{2} & 0 \end{bmatrix} \tag{35}$$

$$B = \begin{bmatrix} -\frac{1}{L-M} & 0 & 0 & 0 \\ 0 & -\frac{1}{L-M} & 0 & 0 \\ 0 & 0 & -\frac{1}{L-M} & 0 \\ 0 & 0 & 0 & -\frac{1}{L-M} \end{bmatrix} \quad (36)$$

$$C = \begin{bmatrix} -\frac{1}{L-M} & 0 & 0 \\ 0 & -\frac{1}{L-M} & 0 \\ 0 & 0 & -\frac{1}{L-M} \\ 0 & 0 & 0 \end{bmatrix} \quad (37)$$

$$u = [v_{ast} \quad v_{bst} \quad v_{cst} \quad T_l]^t \quad (38)$$

$$e = [e_a \quad e_b \quad e_c]^t \quad (39)$$

4. CONTROL STRATEGY

A proportional-integral (PI) controller is a type of feedback controller commonly used in control systems to maintain a desired output by adjusting the input. It combines two control actions: proportional (P) and integral (I).

- Proportional control (P): The proportional part of the controller generates an output that is directly proportional to the current error, which is the difference between the desired set point and the actual process variable. This helps to reduce the overall error quickly. However, a proportional controller alone may not completely eliminate the steady-state error [20].
- Integral control (I): The integral part of the controller sums the error over time, correcting any accumulated offset that the proportional action alone could not eliminate. This action helps to eliminate the steady-state error, ensuring the output eventually matches the desired set point [24].

$$C(t)=Kp[e(t)+(1/\tau i)\int edt] \quad (40)$$

$$C(s)=Kp(1+1/\tau is) \quad (41)$$

Figure 5 represents a proportional-integral (PI) control system, often used in control systems for managing error signals and ensuring the desired output is achieved. W_e and T_e^* represents input error signal and the final output, respectively. The gain *K* corresponds to the steady state value of the output Css [25]. The value of Kp, τi of the controllers can then be calculated as below:

$$Kp=1.2(T/L) \quad (42)$$

$$\tau i=2L \quad (43)$$

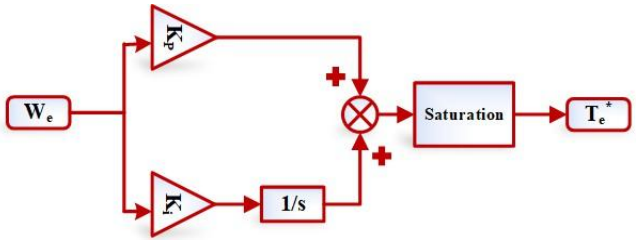

Figure 5. Proportional and integral gain

5. RESULTS AND DISCUSSION

Figure 6 shows the voltage outputs from the PV panel, battery, and DC link without and with a PI controller, where the temperature is kept at 25 °C, and the irradiation ranges from 0 to 1000 W/m^2. From Figure 6(a), it is noted that the PV panel voltage is less than 30 V in the absence of a PI controller. As shown in Figure 6(b) with the PI controller, it is noted that the buck-boost converter boosts the PV panel's output voltage

to higher than 40 V, and feeds it to the battery so that it can be charged. The use of the PI controller also led to an increase in the battery voltage.

Figure 7 shows the output current of the photovoltaic module, battery, and diode without and with a PI controller, where the temperature is kept at 25 °C, and the irradiation ranges from 0 to 1000 W/m^2.Without a PI controller, there are fluctuations in the battery current during charging and discharging. Figure 7 shows the current outputs of the photovoltaic module, battery, and diode without and with a PI controller. As seen in Figure 7(a), when the battery is being charged using a PI controller, the battery current will reach 18 A, while the PV panel's output current is only-35 A. Figure 7(b) shows the variation of PV panel and battery current without controller we can observe that the battery current is about 12 A. By using a PI controller, the fluctuations are reduced, and the current reaches the desired value

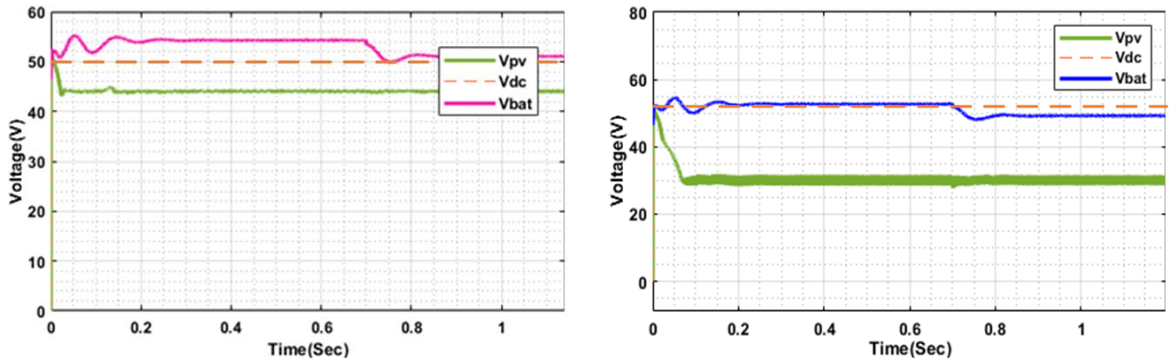

Figure 6. The variation in the voltage of the PV panel, battery (a) without PI and (b) with PI controller

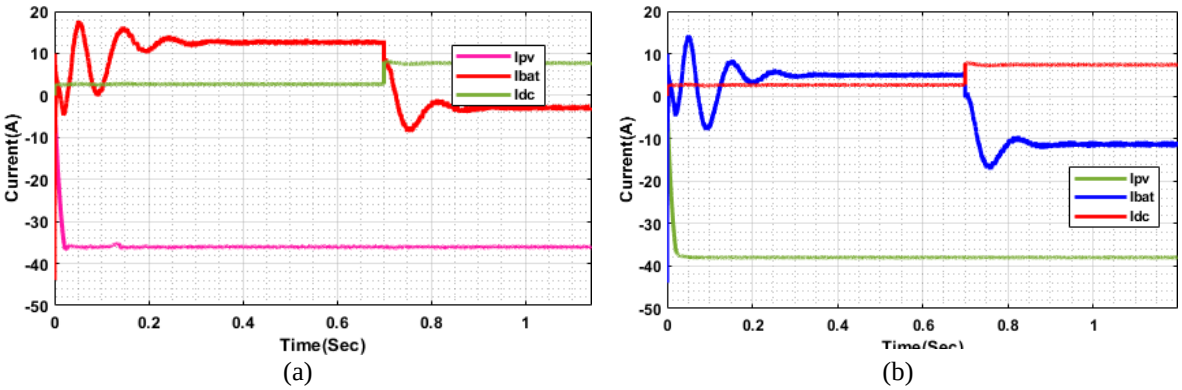

Figure 7. Variation of PV and battery current (a) without PI and (b) with PI controller

The power variation without and with the PI controller is shown in Figures 8(a) and 8(b). Figure 8(a) illustrates that the absence of a PI controller in the system results in noticeable ripples in the PV panel's output power, which leads to increased power loss. Figure 8(b) shows that the PV panel's output power ripples are reduced by the PI controller at the output, and there is also less power loss than without the PI controller. The variation of state of charge (SoC) without and with PI controller is shown in Figures 9(a) and 9(b). It is observed that during charging mode, the SoC of the battery is increased proportionally in both cases, but after 0.7 sec, there is a variation in discharging mode. It discharges fast without a PI controller, whereas the discharge is very slow and less with a PI controller.

The output voltage variation of the converter without a PI controller and with a PI controller is shown in Figures 10(a) and 10(b). The PV panel with MPPT can produce an output voltage of around 40 V and a power of more than 800 W when exposed to different radiation levels between 0 W/m^2 and 1000 W/m^2 at a temperature of 25 °C. These results are displayed in Figure 10. The buck-boost converter will enhance the output voltage from 40 V to 220 V. A charge controller feeds this voltage to the battery. VSI is supplied by a battery to provide an AC voltage that powers the BLDC motor.

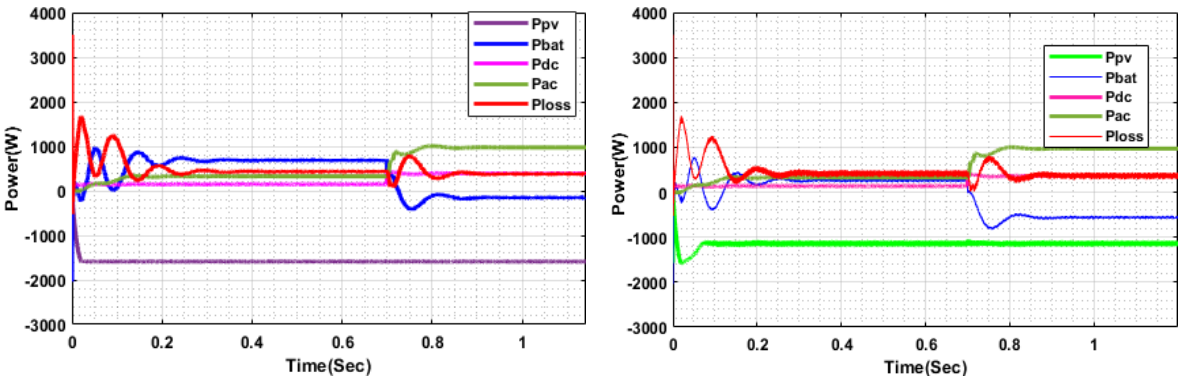

Figure 8. The power variation (a) without PI and (b) with PI controller

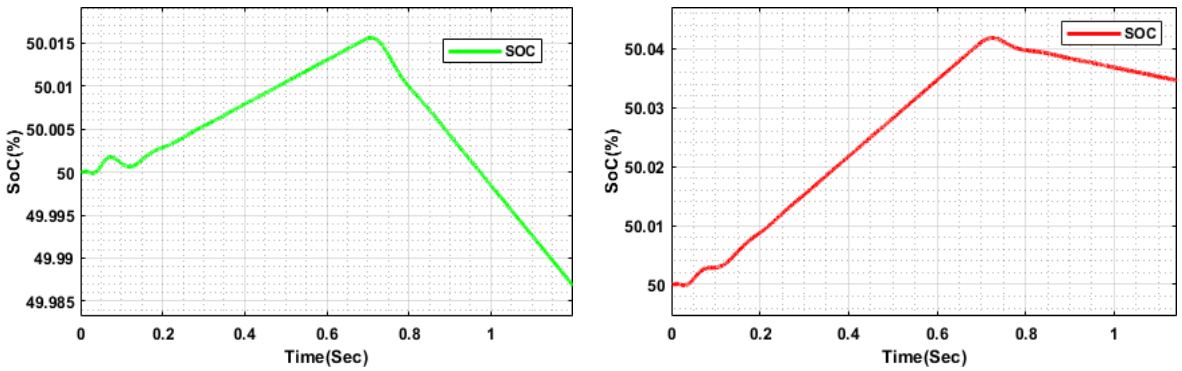

Figure 9. The SoC variation of the battery (a) without PI and (b) with PI controller

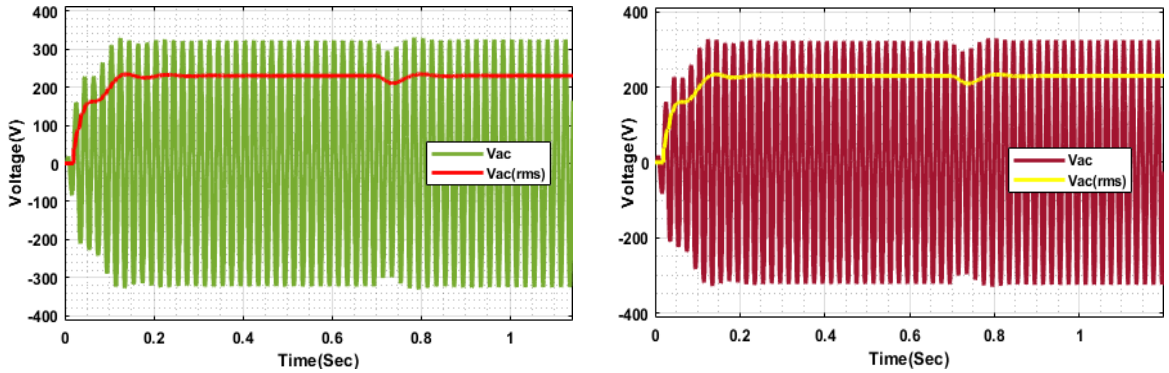

Figure 10. The output voltage variation of the converter (a) without PI and (b) with PI controller

The speed response of the driving system without a PI and with a PI controller at no load and 50% load condition. At no load, the speed response of the BLDC motor driving system without PI and with a PI controller is shown in Figure 11. It is noticeable that the motor reaches a constant speed of 3000 rpm in 0.25 seconds. Overshoot and speed ripple occur in the absence of a PI controller. Additionally, it was seen that without a PI controller, the rise time increases until it settles down to the rated speed.

At 50% full load, the speed response of the BLDC motor driving system without a PI controller and with a PI controller is shown in Figure 11. It is noticeable that the motor reaches a constant speed of 3000 rpm at a time equal to 0.15 seconds. By applying the load at 0.05 sec speed is decreased for both with and without a PI controller. There are slight overshoots and undershoots in both without and with the PI controller. The PI controller has led to an improved rise time and reduced peak overshoot in the speed

response. The variation of efficiency of the proposed system without PI and with PI controller is shown in Figures 12(a) and 12(b). It is evident from Figure 12 that the suggested system achieves an efficiency of 80%. Here, the difference between the PV panel's output power and the ideal output power is used to compute the efficiency. The efficiency of the system is improved with a PI controller.

Table 1 shows the performance comparison between the system without a PI controller and with a PI controller. Without the PI controller, the system has a rise time of 520 ms, whereas with the PI controller, the rise time reduces to 450 ms, indicating a faster response to reach the desired value. The overshoot also decreases from 14% to 12%, which improves system stability and reduces stress on the motor. Similarly, torque ripple is reduced from 18% to 14%, resulting in smoother motor operation, less vibration, and reduced mechanical wear. In addition, the overall efficiency increases from 78% to 84% with the PI controller, showing better utilization of input power and reduced losses. Use of a PI controller enhances response speed, stability, smoothness of operation, and energy efficiency of the system.

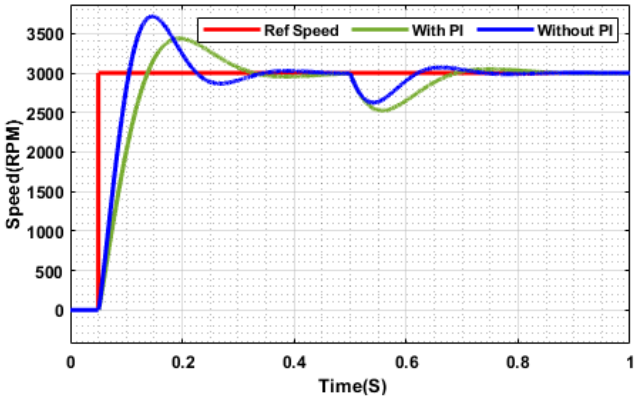

Figure 11. Speed response without PI and with PI controller at no load and load conditions

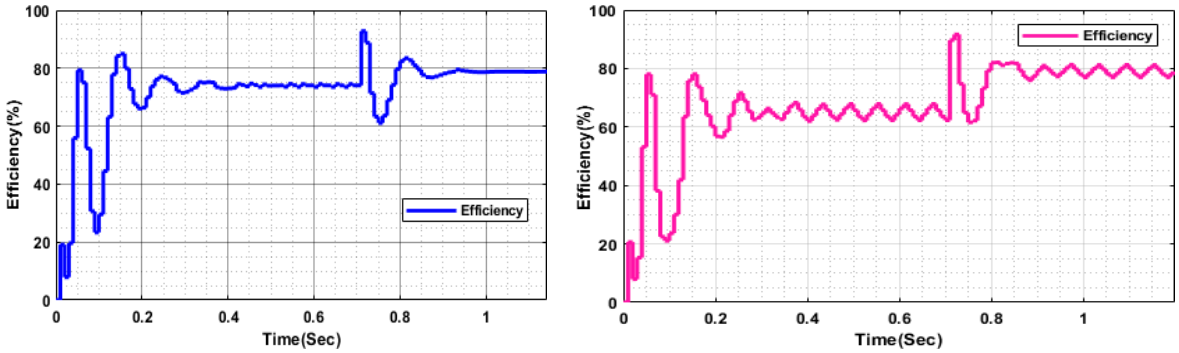

Figure 12. Efficiency of the proposed system (a) without PI and (b) with PI controller

Table 1. Comparison of dynamic performance using different controllers

Controller	Rise time (ms)	Overshoot (%)	Torque ripple (%)	Efficiency (%)
Without PI	520	14	18	78
With PI	450	12	14	84

6. CONCLUSION

The design and improvement of the dynamic performance of a solar-powered brushless DC (BLDC) motor drive system for electric vehicles (EVs) utilized in agricultural applications are effectively demonstrated in this paper. An economic and ecological energy supply is ensured by integrating a solar photovoltaic (PV) system, which lessens environmental impact and dependency on traditional fuels. Under various load and irradiation settings, the BLDC motor demonstrated enhanced torque responsiveness, decreased speed variations, and increased efficiency thanks to the suggested control technique. Solar-powered electric vehicles (SPEVs) generate electricity using photovoltaic (PV) panels. A BLDC motor drive's speed is controlled by a PI controller, and the controller's performance is examined with other

parameters like PV power, battery power, and inverter power. This study describes the modeling and simulation of the complete driving system. Performance prediction over several operational settings serves as an indicator of the model's effectiveness. Using MATLAB/Simulink, the efficiency of the system with and without a PI controller is compared. The suggested system performs better in terms of control than it did without the PI controller. Fully relying on solar energy has certain drawbacks as well, such as a restricted range and a high initial cost. However, they can be avoided by carrying out additional studies in this field utilizing certain intelligent controllers and by using extremely effective solar cells, which have an efficiency of 30–35%. SPEVs in the future will be more functional. In order to further optimize performance and guarantee scalability for large-scale agricultural deployment, future work may concentrate on integrating sophisticated intelligent control algorithms like adaptive neuro-fuzzy or fractional-order controllers and real-time implementation on hardware prototypes.

FUNDING INFORMATION

Authors state no funding involved.

AUTHOR CONTRIBUTIONS STATEMENT

This journal uses the Contributor Roles Taxonomy (CRediT) to recognize individual author contributions, reduce authorship disputes, and facilitate collaboration.

Name of Author	C	M	So	Va	Fo	I	R	D	O	E	Vi	Su	P	Fu
Savitri Medegar	✓	✓	✓	✓	✓	✓		✓	✓	✓			✓	
M. Sasikala		✓							✓	✓	✓	✓		

C : **C**onceptualization
M : **M**ethodology
So : **So**ftware
Va : **Va**lidation
Fo : **Fo**rmal analysis
I : **I**nvestigation
R : **R**esources
D : **D**ata Curation
O : Writing - **O**riginal Draft
E : Writing - Review & **E**diting
Vi : **Vi**sualization
Su : **Su**pervision
P : **P**roject administration
Fu : **Fu**nding acquisition

CONFLICT OF INTEREST STATEMENT

Authors state no conflict of interest.

DATA AVAILABILITY

The data that support the findings of this study are available on request from the corresponding author, [SM]. The data, which contain information that could compromise the privacy of research participants, are not publicly available due to certain restrictions.

REFERENCES

[1] H. El Hafdaoui and A. Khallaayoun, "Mathematical modeling of social assessment for alternative fuel vehicles," *IEEE Access*, vol. 11, pp. 59108–59132, 2023, doi: 10.1109/ACCESS.2023.3284844.

[2] R. Kumar, "Back-EMF-based multiloop sensorless control of solar PV-powered brushless DC motor drive for sustainable agriculture," *IEEE Journal of Emerging and Selected Topics in Industrial Electronics*, vol. 6, no. 4, pp. 1635–1647, Oct. 2025, doi: 10.1109/JESTIE.2025.3601169.

[3] J. Heeraman, R. Kalyani, and B. Amala, "Towards a sustainable future: Design and fabrication of a solar-powered electric vehicle," *IOP Conference Series: Earth and Environmental Science*, vol. 1285, no. 1, p. 012035, Jan. 2024, doi: 10.1088/1755-1315/1285/1/012035.

[4] R. Katuri and S. Gorantla, "Design and comparative analysis of controllers implemented to hybrid energy storage system based solar-powered electric vehicle," *IETE Journal of Research*, vol. 69, no. 7, , 2023, doi: 10.1080/03772063.2021.1941328.

[5] H. M. Khalid *et al.*, "Dust accumulation and aggregation on PV panels: An integrated survey on impacts, mathematical models, cleaning mechanisms, and possible sustainable solution," *Solar Energy*, vol. 251, 2023, doi: 10.1016/j.solener.2023.01.010.

[6] F. Hajiahmadi, M. Jafari, and M. Reyhanoglu, "Machine learning-based control of autonomous vehicles for solar panel cleaning systems in agricultural solar farms," *AgriEngineering*, vol. 6, no. 2, 2024, doi: 10.3390/agriengineering6020081.

[7] M. R. Zaman, M. R. Hoque, M. R. Zaman, and M. S. Ali, "An intensive analysis of the energy management system for hybrid electric vehicles and electric drive system powered by renewable energy sources," *Control Systems and Optimization Letters*, vol. 2, no. 1, 2024.

[8] A. R. Sagor, T. M. Mridul, M. M. H. Bhuiyan, F. A. Mridha, M. R. Hazari, and M. A. Rahman, "Design and implementation of solar PV operated e-power tiller," in *2023 3rd International Conference on Robotics, Electrical and Signal Processing Techniques (ICREST)*, Jan. 2023, pp. 368–373. doi: 10.1109/ICREST57604.2023.10070045.

[9] H. A. Kazem, A. H. A. Al-Waeli, M. T. Chaichan, K. Sopian, A. S. Al Busaidi, and A. Gholami, "Photovoltaic-thermal systems applications as dryer for agriculture sector: a review," *Case Studies in Thermal Engineering*, vol. 47, p. 103047, Jul. 2023, doi: 10.1016/j.csite.2023.103047.

[10] Mohd Azri Abd Aziz *et al.*, "A review on BLDC motor application in electric vehicle (EV) using battery, supercapacitor and hybrid energy storage system: efficiency and future prospects," *Journal of Advanced Research in Applied Sciences and Engineering Technology*, vol. 30, no. 2, pp. 41–59, Apr. 2023, doi: 10.37934/araset.30.2.4159.
[11] N. Prabhu, R. Thirumalaivasan, and B. Ashok, "Critical review on torque ripple sources and mitigation control strategies of BLDC motors in electric vehicle applications," *IEEE Access*, vol. 11, pp. 115699–739, 2023, doi: 10.1109/ACCESS.2023.3324419.
[12] V. Kumarasamy, V. KarumanchettyThottam Ramasamy, G. Chandrasekaran, G. Chinnaraj, P. Sivalingam, and N. S. Kumar, "A review of integer order PID and fractional order PID controllers using optimization techniques for speed control of brushless DC motor drive," *International Journal of System Assurance Engineering and Management*, vol. 14, no. 4, pp. 1139–1150, Aug. 2023, doi: 10.1007/s13198-023-01952-x.
[13] F. Mahmouditabar, A. Vahedi, and N. Takorabet, "Robust design of BLDC motor considering driving cycle," *IEEE Transactions on Transportation Electrification*, vol. 10, no. 1, pp. 1414–1424, Mar. 2024, doi: 10.1109/TTE.2023.3285650.
[14] R. Heidari and J.-W. Ahn, "Torque ripple reduction of BLDC motor with a low-cost fast-response direct DC-link current control," *IEEE Transactions on Industrial Electronics*, vol. 71, no. 1, pp. 150–159, Jan. 2024, doi: 10.1109/TIE.2023.3247732.
[15] H. Wang, K. T. Chau, W. Liu, and S. M. Goetz, "Design and control of wireless permanent-magnet brushless DC motors," *IEEE Transactions on Energy Conversion*, vol. 38, no. 4, pp. 2969–2979, Dec. 2023, doi: 10.1109/TEC.2023.3292178.
[16] I. Anshory *et al.*, "Optimization DC-DC boost converter of BLDC motor drive by solar panel using PID and firefly algorithm," *Results in Engineering*, vol. 21, p. 101727, Mar. 2024, doi: 10.1016/j.rineng.2023.101727.
[17] T. Shukla and S. Nikolovski, "A solar photovoltaic array and grid source-fed brushless DC motor drive for water-pumping applications," *Energies*, vol. 16, no. 17, p. 6133, Aug. 2023, doi: 10.3390/en16176133.
[18] M. Karthika and K. C. R. Nisha, "Arithmetic optimization algorithm-based torque ripple minimization technique for solar fed sensorless BLDC drive for domestic applications," *Optik*, vol. 290, p. 171286, Oct. 2023, doi: 10.1016/j.ijleo.2023.171286.
[19] P. Mandre, B. Somanna, S. Gupta, and S. Nema, "ANN based solar MPPT for BLDC motor load using bidirectional converter," in *2023 IEEE International Students' Conference on Electrical, Electronics and Computer Science (SCEECS)*, Feb. 2023, pp. 1–6. doi: 10.1109/SCEECS57921.2023.10061821.
[20] A. Sen and B. Singh, "Solar powered position sensor free PMBLDC motor drive with dynamic observer control," *IEEE Journal of Emerging and Selected Topics in Industrial Electronics*, vol. 5, no. 2, pp. 450–461, Apr. 2024, doi: 10.1109/JESTIE.2023.3331229.
[21] S. Parvathy, C. B. C. Kumar, P. H. H. Krishna, C. S. Prakash, and K. V. R. Kumar, "Design and implementation of PV-fed BLDC motor for irrigation scheme," in *2024 Second International Conference on Emerging Trends in Information Technology and Engineering (ICETITE)*, Feb. 2024, pp. 1–6. doi: 10.1109/ic-ETITE58242.2024.10493803.
[22] N. Kalaiselvan, T. S. Umesh Kumar, and S. Neelkamal, "Integrating BLDC motor in solar EVs: design, modeling, and fault identification," in *2024 3rd International Conference on Artificial Intelligence For Internet of Things (AIIoT)*, May 2024, pp. 1–5. doi: 10.1109/AIIoT58432.2024.10574583.
[23] S. BalaKumar, M. Lemma, and M. Godato, "Solar-powered ANN-based MPPT with zeta converter for BLDC motor water pumping in rural Ethiopia for sustainable agriculture," *Discover Sustainability*, vol. 6, no. 1, 2025, doi: 10.1007/s43621-025-00893-8.
[24] G. J. Sagar, V. Badrinath, V. V. Nag, S. Nagalingam, P. Mishra, and T. Mahto, "Enhancement of permanent magnet synchronous motor drive-based solar-powered electric vehicle drivetrain," in *2025 International Conference on Sustainable Energy Technologies and Computational Intelligence (SETCOM)*, Feb. 2025, pp. 1–5. doi: 10.1109/SETCOM64758.2025.10932442.
[25] R. Hemalatha, S. V. Keshika, and A. Roopika, "Modeling and simulation of control of BLDC motor for quadcopter using solar power," in *Universal Threats in Expert Applications and Solutions*, 2026, pp. 391–402. doi: 10.1007/978-981-96-7289-9_31.

BIOGRAPHIES OF AUTHORS

Savitri Medegar is currently working as an assistant professor in the Department of Electrical and Electronics Engineering at the Faculty of Engineering and Technology Exclusively for Women, Kalaburagi. Pursuing Ph.D. in power electronics from Sharnbasva University (SUK). Her research interests include electric vehicles, power electronics, and renewable energy resources. She has over 10 years of teaching and research experience and has published more than 5 papers in reputed national and international journals and conferences. She has one patent and two grants. She can be contacted at email: savtri.m@sharnbasvauniversity.edu.in.

M. Sasikala received a B.E. in Electrical Engineering from University College of Engineering, Osmania University, Hyderabad, in 1985 with First Class Distinction, followed by an M.E. in Power Systems from the same institution in 1987, earning a gold medal for securing the top rank in the university. Completed a Ph.D. in Electrical Engineering from Jawaharlal Nehru Technological University (JNTU), Hyderabad, in 2008. With over 32 years of teaching and research experience, academic roles have included serving as Professor and Principal in various institutions since 2008, currently associated with Sharnbasva University, Kalaburagi, since 2014. Research interests include power systems, electric drives, intelligent control systems, and renewable energy applications. Published 55 research papers in reputed national and international journals and presented 26 papers at conferences in India and abroad. Successfully guided seven Ph.D. candidates, with four more currently under supervision. Contributions extend to serving as a Reviewer for several international journals, editing a book chapter, and actively participating as a Board of Studies (BOS) and Board of Examiners (BOE) member, an Academic Council Member at Sharnbasva University, and a doctoral committee member for multiple universities. Additionally, served as an advisor for the UPSC examination. She can be contacted at email: sasi_mun@rediffmail.com.